This is an original manuscript of an article published by Taylor & Francis Group in Molecular Physics on 05 Jun 2017, available online: https://doi.org/10.1080/00268976.2017.1340682

Viscosity and normal stress forces of Lennard Jones chains using reverse non-equilibrium Molecular Dynamics

Patsy V. Ramírez-González[1*], Vladimir Alonso Escobar-Barrios[1]

[1] *Instituto Potosino de Investigación Científica y Tecnológica, Camino a la Presa de San José 2055, Lomas 4a Sección, San Luis Potosí, San Luis Potosí, C.P. 78216, México.*

**corresponding author: patsy.ramirez@ipicyt.edu.mx*

Keywords: Viscosity, viscoelasticity, normal stress forces, non-equilibrium molecular dynamics, Lennard-Jones potential

Abstract

Reverse non-equilibrium molecular dynamics was applied for the calculation of the viscosity for different chain lengths. Each chain consisted of *m* tangent spherical sites, where *m* was 1, 2, 4, 8, or 16 respectively. From these results, shear thinning was observed at high shear rates. The normal stress forces were also estimated via the calculation of the total stress tensor, and they were related to the shear thinning effect depending on the length of the chain. Furthermore, a power law equation was used to fit the rheological curves of each chain, making possible the calculation of the viscoelasticity as a function of the sites involved in the chains.

1. Introduction

Liquid viscosity is one of the most measured transport properties in chemical and petrochemical process designs. Nevertheless, no large experimental data are always available for all the fluids. The viscosity can be determined at the macroscopic level by the constitutive equation of Newton's law of viscosity, which relates the shear stress to the shear rate.[1] Several methods are available for calculating shear viscosities of liquids at macroscopic level, for example the friction theory.[2-5] At the microscopic level, the viscosity is obtained due to the momentum transfer between fluid layers moving at different speed. In this sense, viscosity can be calculated with equilibrium methods that make use of molecular dynamics (MD) simulation, which are based on pressure or momentum fluctuation. The Green-Kubo (GK) expression for the shear viscosity is given by integration of the pressure autocorrelation function.[6-8]There are also alternative methods that are carried out with non-equilibrium molecular dynamics (NEMD) simulations.[9-10] A nonequilibrium system can be modelled as a perturbed ensemble. The perturbed field is added to the statistical mechanical description, which works on the system preventing it to relax to equilibrium and measures the resulting flux. The work is converted to heat, and the heat must be removed in order to obtain a well-defined steady state. Therefore, thermostats will also need to be included in the statistical mechanical model.[8, 11] NEMD has been successfully applied to study the microscopic origin of the nonlinear viscoelastic properties of polymer melts.[12] However, it may require long simulations due to relatively large fluctuations in the pressure tensor.

There is another method used in cases where the flux is difficult to define microscopically or is slowly converging. In contrast to equilibrium methods and NEMD, the reverse non-equilibrium molecular dynamics (RNEMD) proposed by Müller[13-15]conserves the total energy as well as the total linear momentum, so it can be used in a microcanonical ensemble without an additional thermostat. There is viscous heating but the excess heat is drained by the momentum exchange itself. It acts as an internal thermostat, i.e., a mechanism that removes the heat generated by friction. This method imposes the hard-to-measure flux, J_{xy}, and computes the resulting easy-to-measure shear field, $\dot{\gamma}$.

Once knowing the flux and the shear field values, the viscosity can be calculated using Newton's law of viscosity[1]:

$$\boldsymbol{\eta} = -\frac{\boldsymbol{J_{xy}}}{\dot{\boldsymbol{\gamma}}} \quad (1)$$

When a fluid is at rest, it can support only a uniform normal stress, $T_{11} = T_{22} = T_{33}$, where T_{ij} is one component of the stress tensor. This normal stress is called the hydrostatic pressure p.[1] Thus, for a fluid at rest, the stress tensor is:

$$\mathrm{T} = \begin{bmatrix} -\boldsymbol{p} & \mathbf{0} & \mathbf{0} \\ \mathbf{0} & -\boldsymbol{p} & \mathbf{0} \\ \mathbf{0} & \mathbf{0} & -\boldsymbol{p} \end{bmatrix} = -\boldsymbol{p} \begin{bmatrix} \mathbf{1} & \mathbf{0} & \mathbf{0} \\ \mathbf{0} & \mathbf{1} & \mathbf{0} \\ \mathbf{0} & \mathbf{0} & \mathbf{1} \end{bmatrix} \quad (2)$$

where the minus sign is used because compression is usually considered to be negative. can also be written as:

$$\mathrm{T} = -\boldsymbol{p}\mathrm{I} \quad (3)$$

When working with fluids in motion (under shear rate) the total stress tensor is the sum of two parts:

$$\mathrm{T} = -\boldsymbol{p}\mathrm{I} + \tau \quad (4)$$

where τ is known as the viscous stress tensor. For a Newtonian incompressible fluid, the only normal stress in steady shear is the hydrostatic pressure, then:

$$\mathrm{T} = -\boldsymbol{p} \begin{bmatrix} \mathbf{1} & \mathbf{0} & \mathbf{0} \\ \mathbf{0} & \mathbf{1} & \mathbf{0} \\ \mathbf{0} & \mathbf{0} & \mathbf{1} \end{bmatrix} + \begin{bmatrix} \mathbf{0} & \boldsymbol{\tau_{xy}} & \mathbf{0} \\ \boldsymbol{\tau_{yx}} & \mathbf{0} & \mathbf{0} \\ \mathbf{0} & \mathbf{0} & \mathbf{0} \end{bmatrix} \quad (5)$$

The value of τ_{xy} for a Newtonian fluid must be the same as the value of the flux J_{xy} in Equation 1. When working with non-Newtonian fluids, the normal stress components in viscous tensor is no longer zero. In this work, it will be demonstrated that for large chains, the fluid becomes non-Newtonian and the normal stress components take major importance.

2. Theory

For the site–site interaction potential a truncated Lennard-Jones (LJ) potential was used:

$$\boldsymbol{U_{LJ}} = \begin{cases} \boldsymbol{4\varepsilon}\left[\left(\frac{\boldsymbol{\sigma}}{\boldsymbol{r}}\right)^{\mathbf{12}} - \left(\frac{\boldsymbol{\sigma}}{\boldsymbol{r}}\right)^{\mathbf{6}}\right] & \text{if } r < r_{cutoff} \\ \mathbf{0} & \text{if } r \geq r_{cutoff} \end{cases} \quad 6)$$

where ε is the energy constant (or well depth), σ is the diameter of the atom, and r is the site–site separation. If r is larger than the cut-off radio, r_{cutoff}, the potential is equal to zero. The cutoff distance was set to 2.5σ. For epsilon and sigma, the common values of argon were used, namely ε/k_B = 119.8 K and σ = 0.3405 nm, where k_B is the Boltzmann constant.

A chain is defined as a molecule of m atoms joined by a strong harmonic bond modeled as a simple spring-type potential:[16]

$$\boldsymbol{U_{bond}} = -\frac{\mathbf{1}}{\mathbf{2}}\boldsymbol{k}(\boldsymbol{r} - \boldsymbol{\sigma})^{\mathbf{2}} \quad 7)$$

where k is the spring constant equal to $3000\ \varepsilon/\sigma^2$, as proposed by Johnson et al.[16] In this work, the formed chains consisted of m tangent spherical sites, where m was 1, 2, 4, 8, or 16. No bond angle deformation or torsion potentials were used, i.e., the chains were fully flexible.

Throughout this work, reduced (dimensionless) properties were used:

$t^* = \frac{t}{\sigma}\sqrt{\frac{\varepsilon}{m_p}}$, $T^* = \frac{k_B T}{\varepsilon}$, $\rho^* = \sigma^3\rho$, $P^* = \frac{P\sigma^3}{\varepsilon}$, $\eta^* = \eta\frac{\sigma^2}{\sqrt{m_p\varepsilon}}$, $\tau^* = \frac{\tau\sigma^3}{\varepsilon}$, $\dot{\gamma}^* = \frac{\dot{\gamma}\sigma^2}{\varepsilon}$, $N^* = \frac{N\sigma^3}{\varepsilon}$

where t is the time, m_p the mass of a particle, T the temperature, ρ the atomic number density, P the pressure, η the viscosity, τ the shear stress, N the normal stress and $\dot{\gamma}$ is the shear rate.

2.1. Reverse non-equilibrium molecular dynamics

The RNEMD method calculates the shear viscosity of a fluid by imposing a nonphysical exchange of momentum and measuring the resulting shear velocity gradient. Based on the algorithm proposed by Müller,[13-15, 17] a simulation box was divided into two halves and subdivided into Z slabs labeled from 1 to Z, see Figure 1.

The purpose of this, is to have the first slab and the Z^{th} slab with the most positive x component of the momentum, and the slab $Z/2$ and $Z/2+1$ with the most negative x component of the momentum. With this scheme, no modification has to be done to periodic boundary conditions and there is no need to introduce artificial walls into the system. The physical and unphysical momentum at the stationary state give rise to a biperiodical velocity profile across the fluid, with a slope between halves with same magnitude but different direction. The advantages of this method is that the total energy and the total linear momentum are conserved and, hence, a thermostat is not needed; also the resulting raw data are well-defined, converge rapidly and the gradients obtained can be easily analyzed.

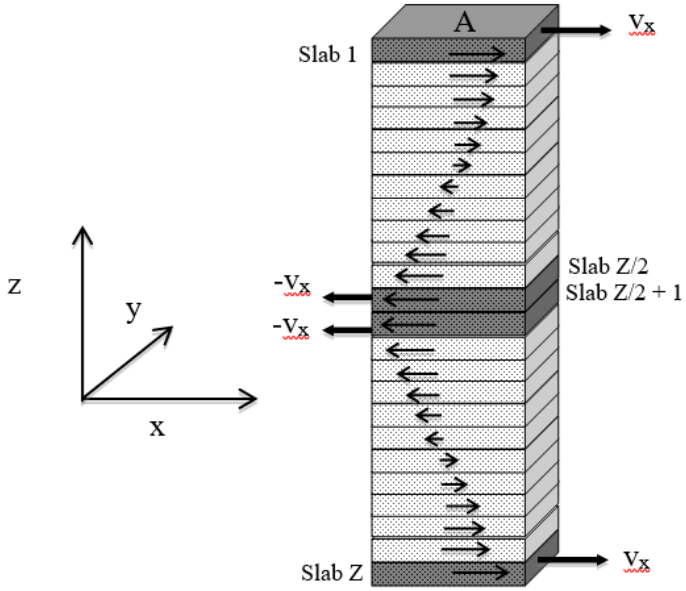

Figure 1. Geometry of the experimental non-equilibrium state.

To achieve the velocity profiles, first the slabs 1 and $Z/2$, which have different velocity directions, are chosen. Then, the atom in slab 1 with the lowest momentum in x direction, $p_{x,1,}$ and the atom in slab $Z/2$ with the greatest momentum in x direction, $p_{x,Z/2}$ are localized and then their values are exchanged. The same is done for the atoms in slab $Z/2+1$ and Z. The atoms must have the same mass, so the total linear momentum and kinetic energy can be conserved. The momenta swaps are carried out every step, so that the total exchanged momentum is:

$$\boldsymbol{p_{tot}} = \sum\left(\boldsymbol{p_{x,1}} - \boldsymbol{p_{x,Z/2}}\right) + \sum\left(\boldsymbol{p_{x,Z/2+1}} - \boldsymbol{p_{x,Z}}\right) \quad 8)$$

and the momentum flux J_{xy} can be calculated as

$$\boldsymbol{J_{xy} = \frac{p_{tot}}{2tA}} \qquad 9)$$

where $A=L_xL_z$ (lengths of the orthorhombic simulation box in the x and z directions), the factor 2 arises because of the periodicity of the system and t is the total time of the simulation that can be calculated by multiplying the step time by the number of time steps. The flow velocity v_x in every slab is calculated as the average of the velocity $v_{x,i}$ of all atoms i in that slab. The velocity profile is approximately linear in each section of Figure 1 and the slope $\boldsymbol{\dot{\gamma} = \frac{\partial v_x}{\partial y}}$ can be obtained by a linear regression.

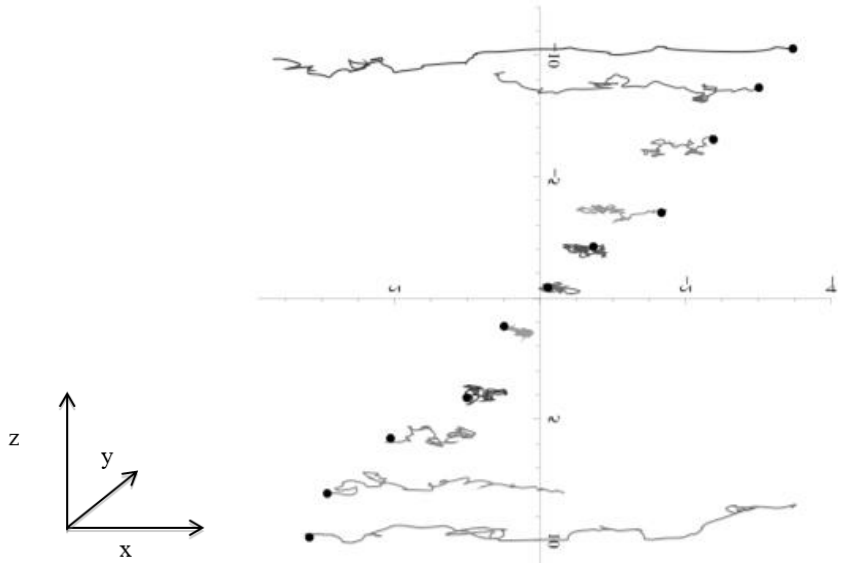

Figure 2. Movement of a particle in a time interval. Formation of a linear velocity profile.

In Figure 2, the real movement path of a particle in the simulation box is observed during a time interval. The particle finishes its movement at the position marked with the point. A formation of a linear velocity profile can be clearly observed. This method works also for molecular fluids if molecules are modeled as entirely flexible and no constraints are used.

2.2. Total stress tensor

According to Equation 5, the total stress tensor T is determined as follows:[18]

$$\mathrm{T} = \begin{pmatrix} \boldsymbol{T_{xx}} & \boldsymbol{T_{xy}} & \boldsymbol{T_{xz}} \\ \boldsymbol{T_{yx}} & \boldsymbol{T_{yy}} & \boldsymbol{T_{yz}} \\ \boldsymbol{T_{zx}} & \boldsymbol{T_{zy}} & \boldsymbol{T_{zz}} \end{pmatrix} \quad 10)$$

where T is equal to Equation 4. Every component of the total stress tensor can be calculated with the sum of the kinetic and potential energy contribution[17,18]:

$$\boldsymbol{T_{\alpha\beta}} = \frac{\mathbf{1}}{\boldsymbol{V}}\left(\sum_{\boldsymbol{i}} \frac{\boldsymbol{p_{i\alpha} p_{i\beta}}}{\boldsymbol{m_p}} + \sum_{\boldsymbol{i}} \sum_{\boldsymbol{j>i}} \boldsymbol{F_{ij}} \frac{\boldsymbol{\alpha_{ij}\beta_{ij}}}{\boldsymbol{r_{ij}}}\right) \quad 11)$$

where V is the volume of the box, α and β can be x, y, or z, $p_{i\alpha}$ and $p_{i\beta}$ are the sum of the particle momentums in α and β directions respectively, r_{ij} is the site–site distance and F_{ij} denotes the forces exerted on atom i by atom j; this force is the result of the summation of the LJ forces and the bond forces. This way, the hydrostatic pressure named in Equation 2 is:

$$\boldsymbol{P_{hyd}} = \frac{\mathbf{1}}{\mathbf{3}}\boldsymbol{Tr}(\mathrm{T}) = \frac{\boldsymbol{T_{xx}+T_{yy}+T_{zz}}}{\mathbf{3}} = \frac{\mathbf{1}}{\boldsymbol{V}}\left(\boldsymbol{nk_B T} + \frac{\mathbf{1}}{\mathbf{3}}\sum_{\boldsymbol{i}} \sum_{\boldsymbol{j>i}} \boldsymbol{F_{ij}}.\boldsymbol{r_{ij}}\right) \quad 12)$$

where n is the total number of atoms, k_B is the Boltzmann constant and T is the temperature. It is very important to remark that the component of the total stress where shear is applied, i.e. T_{xy} is:[18,19]

$$\boldsymbol{T_{xy}} = \frac{\mathbf{1}}{\boldsymbol{V}}\left(\boldsymbol{m_p} \sum_{\boldsymbol{i}}\left[\boldsymbol{v_{iy}}(\boldsymbol{v_{ix}} - \boldsymbol{u_x})\right] + \sum_{\boldsymbol{i}} \sum_{\boldsymbol{j>i}} \boldsymbol{F_{ij}} \frac{\boldsymbol{x_{ij} y_{ij}}}{\boldsymbol{r_{ij}}}\right) \quad 13)$$

This equation is similar to Equation 11 but the stream velocity in x direction, u_x, must be removed from the velocity in x direction, v_x. If the fluid presents Newtonian behavior, T_{xy} must be equal to the calculated flux J_{xy} in Equation 9. But if the fluid presents non-Newtonian behavior, the normal stresses in Equation 5 will not be zero any more. A way to find the value of these normal stresses is to calculate the pressure tensor in equilibrium, i.e., when the fluid is at rest and no shear is applied. Then, from Equation 4 the viscous stress tensor is calculated as:

$$\boldsymbol{\tau} = \mathrm{T} + \boldsymbol{p}\mathrm{I} \qquad 14)$$

The objective of doing this is to consider the normal stresses which are the cause of the non-Newtonian behavior that makes the viscosity decrease.

2.3. Normal stress differences

Normal stress differences are associated with nonlinear effects and are the result of the microstructure no longer anisotropic under flow conditions.[20-22] The normal stresses are considered responsible for various relevant industrial rheological effects as the Weissenberg or 'rod-climbing' effect, the 'die-swell' effect and the post-extrusion effect. A large number of complex fluids such as polymers, colloidal suspensions, micelles, etc. exhibit normal stresses. The total stress in a fluid can be described by:

Shear stress: τ_{xy}

First normal stress difference: $N_1 = \tau_{xx} - \tau_{yy}$

Second normal stress difference: $N_2 = \tau_{yy} - \tau_{zz}$

N_1 provides the axial pressure and N_2 is related to the pressure variation. The second normal stress difference $N2$ is almost always very small in comparison to $N1$, so in this work $N2$ was negligible.

2.4. Simulation Details

The simulation program was developed by the author, and it was already validated for various thermophysical properties.[23] The reduced time step was $\Delta t^* = 0.0023$. The number of molecules were 1000 for m = 1, 800 (1600 atoms) for m = 2, 400 (1600 atoms) for m = 4, 300 (2400 atoms) for m = 8, and 200 (3200 atoms) for m = 16. Verlet algorithm and periodic boundary conditions were used. In order to save CPU time, a Verlet neighbor list was implemented with an outer shell radius of 3.6σ. For all properties standard deviations were computed in order to obtain the statistical errors.

3. Results

The viscosity of a single spherical site was calculated for different temperatures. In Figure 3 it can be observed that viscosity is higher for lower temperatures and decreases

as temperature grows up. It can also be observed that as shear rate increases, the viscosity decreases (shear thinning effect). Viscosity curve obtained from Delhommelle et al.[11] is also shown for a lower temperature and density, and it follows similar behavior of viscosity decrease at the same range of shear rate.

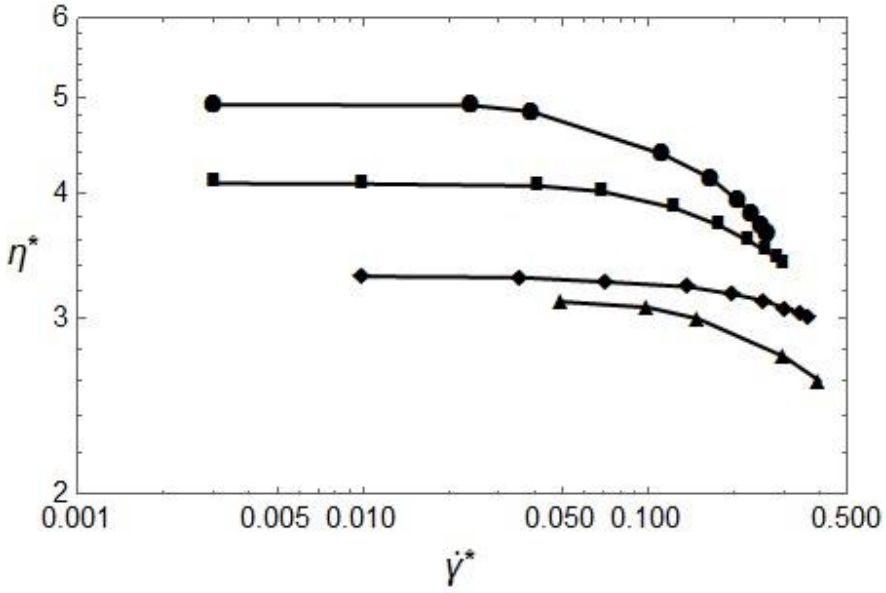

Figure 3. Viscosity as a function of shear rate for m = 1 (□*= 0.9). Different reduced temperatures ●: T*=0.8, ■: T*=1, ♦: T*=1.5. Lines are only for visual guiding. ▲: results from Delhommelle et al.11 for T*= 0.722, m = 1, □*= 0.84.

The viscosity was also calculated for different densities at T^*=2 for m=1 (Figure 4), showing an exponential increment as density increases. Results were compared with the work of other authors and they are in good agreement.

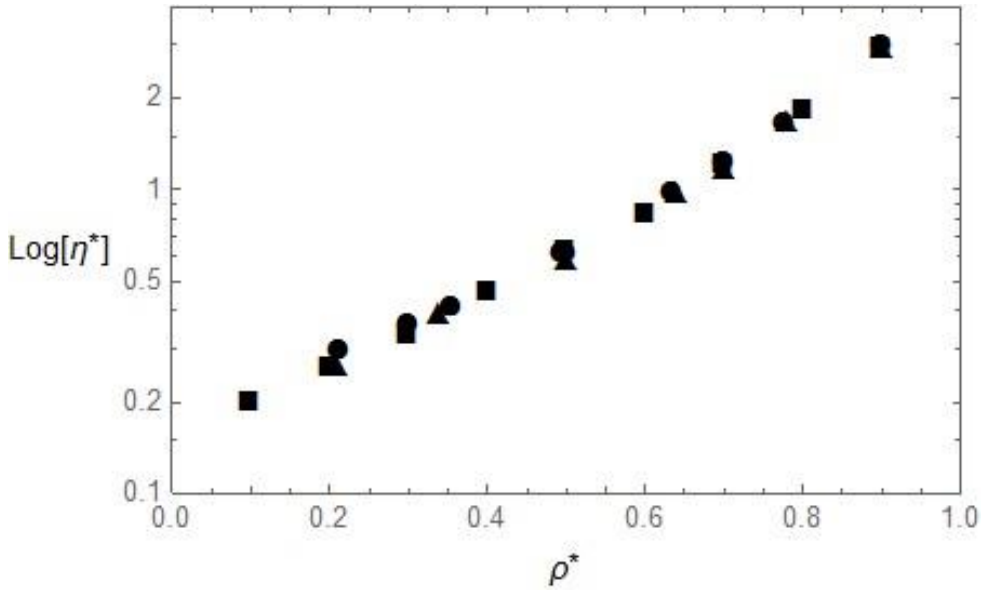

Figure 4. Viscosity for different values of density at T^*=2. ■: this work, ●: results from G. Galliero et al.[24], ▲: results from Llovell et al.[25]

In Figure 5 the viscosity as a function of shear rate for chains of m = 1, 2, 4, 8 and 16 spherical sites is displayed. Figure 5 shows that as long as m increases, the shear thinning effect is more evident (see m=16, filled diamonds), alsowhen m increases, shear thinning appears at lower shear rates.[12, 26] For all values of m viscosity reaches a first Newtonian regime at low shear rates.

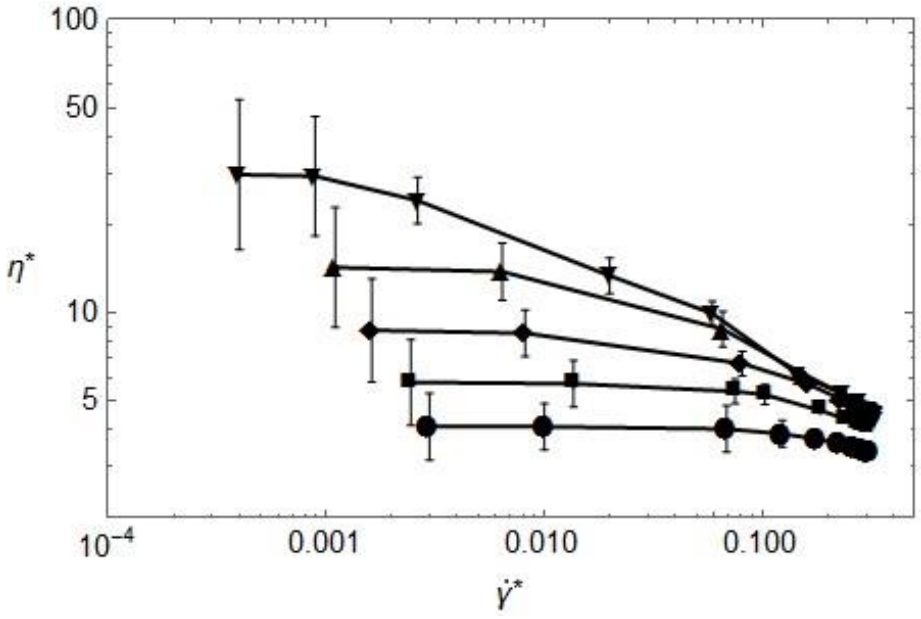

Figure 5. Viscosity as a function of shear rate at T^*=1 and ρ^*= 0.9. ●: m=1, ■: m=2, ♦: m=4, ▲: m=8, ▼: m=16. Lines are only for visual guiding.

The shear thinning effect appears when normal stress forces increase and Equation 5 is no longer zero in the diagonal of the viscous part. To prove this, the total stress tensor was calculated with Equation 11, the hydrostatic pressure of the fluid at rest was calculated with Equation 12 and the viscous stress tensor, τ, was determined with Equation 14 for all the chains at different shear rates. In Equations 15 and 16 an example of the resultant tensor for m=2 at low and high shears rates respectively, is displayed.

$$\boldsymbol{\tau}(\dot{\boldsymbol{\gamma}} = \mathbf{0.1},\ \boldsymbol{m} = \mathbf{2}) = \begin{bmatrix} \mathbf{0.1} & \mathbf{-0.3} & \mathbf{0} \\ \mathbf{-0.3} & \mathbf{0.2} & \mathbf{0} \\ \mathbf{0} & \mathbf{0} & \mathbf{0.2} \end{bmatrix} \quad 15)$$

$$\boldsymbol{\tau}(\dot{\boldsymbol{\gamma}} = \mathbf{0.3},\ \boldsymbol{m} = \mathbf{2}) = \begin{bmatrix} \mathbf{0.3} & \mathbf{-1} & \mathbf{0} \\ \mathbf{-1} & \mathbf{0.6} & \mathbf{0} \\ \mathbf{0} & \mathbf{0} & \mathbf{0.8} \end{bmatrix} \quad 16)$$

It can be observed that for a higher shear rate, the normal components in the diagonal become more relevant in the calculation of the viscous stress tensor. In Figures 6, 7 and 8 the graphical results of the viscosity $\eta*$, the shear stress τ_{xy*} and the normal stress N_{1*} for m=1, m=2 and m=16 respectively, are shown.

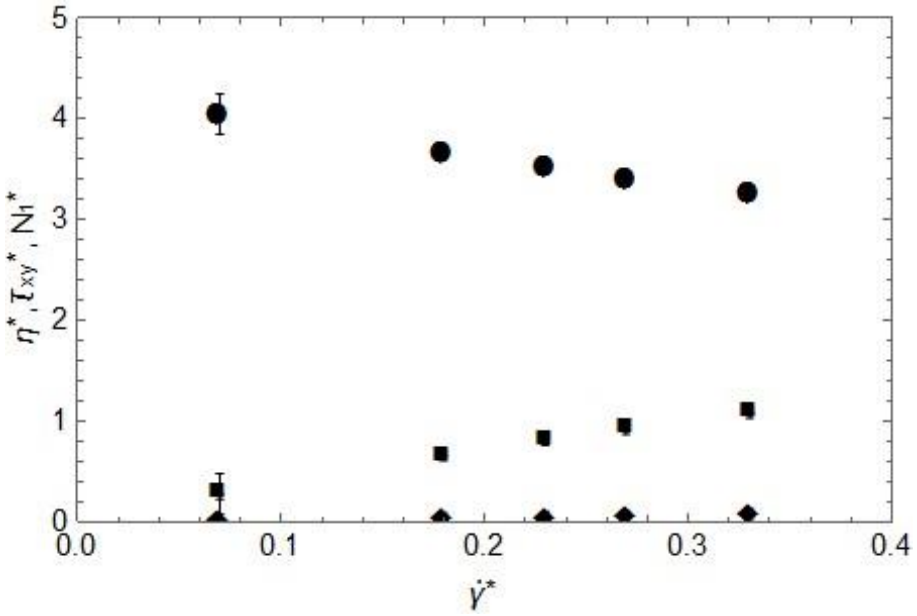

Figure 6. Rheological results for m=1 at T*=1 and ρ*= 0.9 as a function of shear rate. ●: viscosity η*, ■: shear stress τ_{xy}*, ♦: normal stress N_1*.

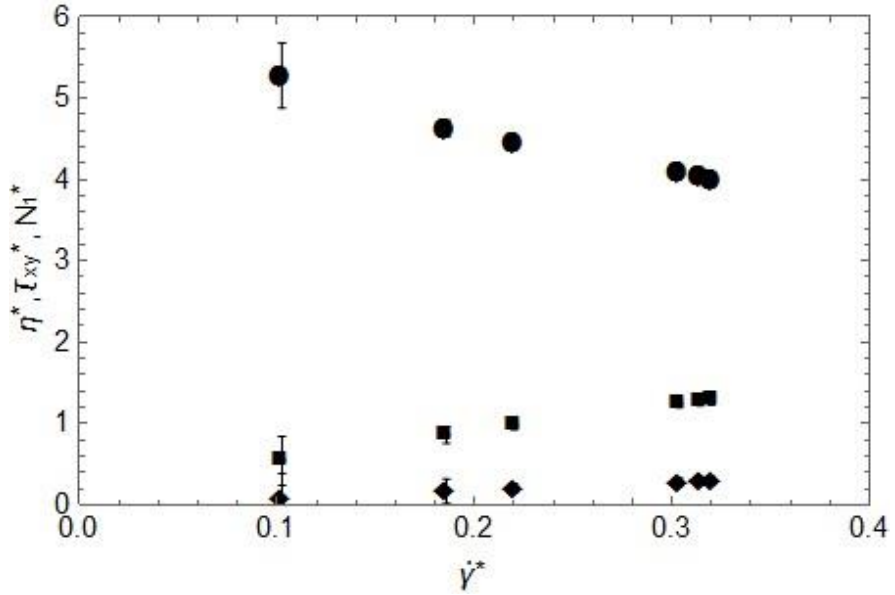

Figure 7. Rheological results for m=2 at T^*=1 and ρ^*= 0.9 as a function of shear rate. ●: viscosity η^*, ■: shear stress τ_{xy}^*, ♦: normal stress N_1^*.

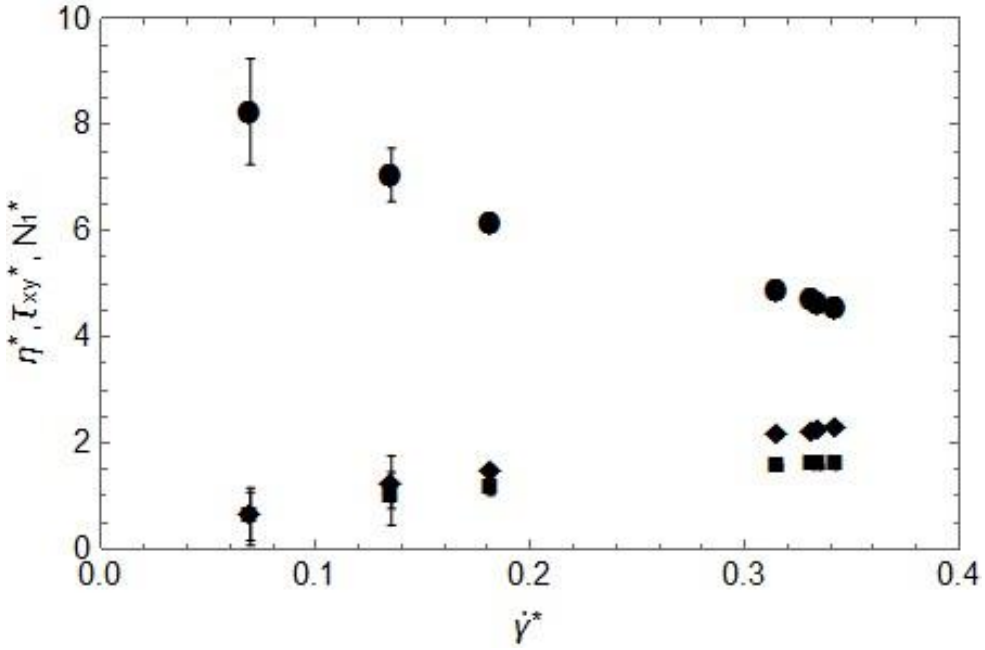

Figure 8. Rheological results for m=16 at T^*=1 and ρ^*= 0.9 as a function of shear rate. ●: viscosity η^*, ■: shear stress τ_{xy}^*, ♦: normal stress N_1^*.

In these graphics, it can be observed that the normal stress grows up as long as chain increases. When m=1, N_1 is almost zero and shear stress controls the movement. In

Figure 7 corresponding to *m*=2, the normal stress is more significant but shear stress still predominate. In the case of *m*=16, the normal stress is higher than shear stress, which means that this fluid is highly viscoelastic.

From a physical point of view, the generation of an unequal normal stress arises from the fact that when applying shear rate, the liquid becomes anisotropic. Namely, the chain molecules, which at rest goes everywhere behave in alignement after shearing. In Figure 9 the simulation box conformed by chains constituted with 16 spherical sites at rest (left) and after shear deformation (right) is shown. The arrow represents the *m*=16 chain from beginning to end (peak of the arrow). It can be observed that molecules at rest goes everywhere, but after deformation they mostly aligne in x direction, the direction from the shear application.

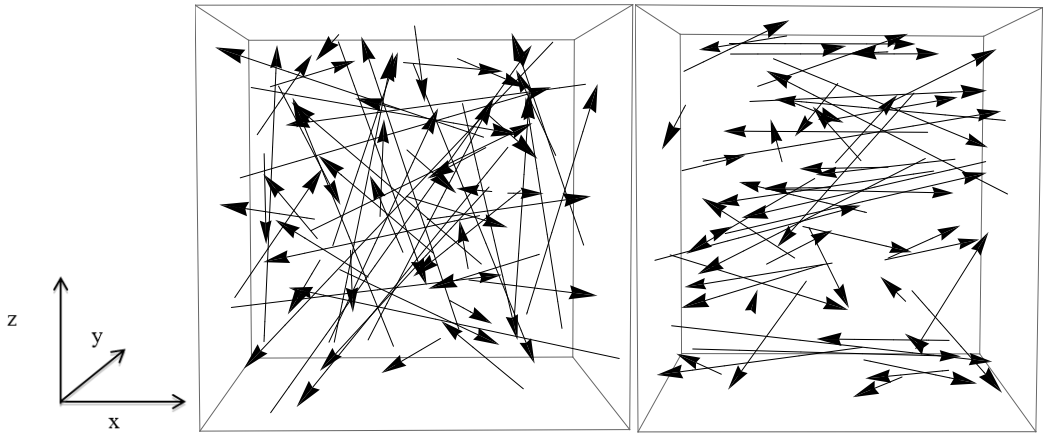

Figure 9. Chains before (left) and during shear deformation (right).

To corroborate the alignment of chains, the radial distribution function was determined. It defines the probability of finding a particle at a determined distance with respect to other reference particle, giving us important structural information. When shear rate is increased, the atoms of the liquid ensemble form structurally arrested states with crystal-like symmetries. [27-28] Shear is able to produce anisotropy, that can be revealed by radial distribution function. In Figure 10.Figure 10, particle's positions are shown for a) non-shear-induced system and b) shear-induced system. It can be observed the difference between them, in the first figure there is an isotropic

system meanwhile in second figure a crystal-like symmetry is formed.

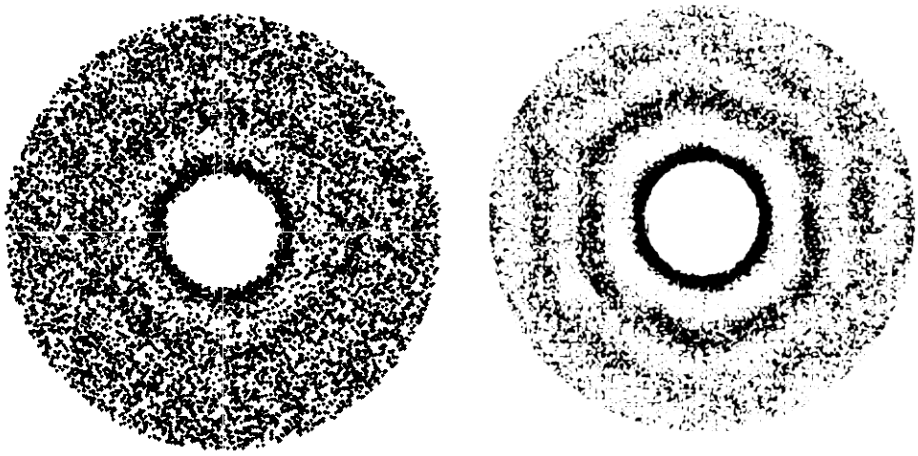

Figure 10. Radial distribution function for a) non-shear-induced system and b) shear-induced system.

The structure of the fluid as well as the normal stress appearance give rise to the shear thinning effect. All the fluids that behave this way are called pseudoplastic or viscoelastic, and many equations or models are available for the description of the fluid's behavior.

Regarding the results of this work, the best equation to fit the rheological behavior of the chains was the Power Law model,[29] which follows the next equation:

$$\boldsymbol{\tau_{xy}} = \boldsymbol{K}\dot{\boldsymbol{\gamma}}^{\boldsymbol{a}} \qquad 17)$$

where *K* is the flow consistency index and *a* the flow behavior index. The inverse of *a* is the so-called pseudoplasticity index, and it indicates how viscoelastic is a fluid. If 1/*a* is equal to 1 it means that the fluid is Newtonian. For the calculation of *a*, the following equation was used:

$$\ln\left(\boldsymbol{\tau_{xy}}\right) = \ln(\boldsymbol{K}) + \boldsymbol{a}\ln(\dot{\boldsymbol{\gamma}}) \qquad 18)$$

The value of *a* and 1/*a* was calculated for all the chains. In Figure 11 a plot of the pseudoplasticity index as a function of the number of atoms in chain is displayed.

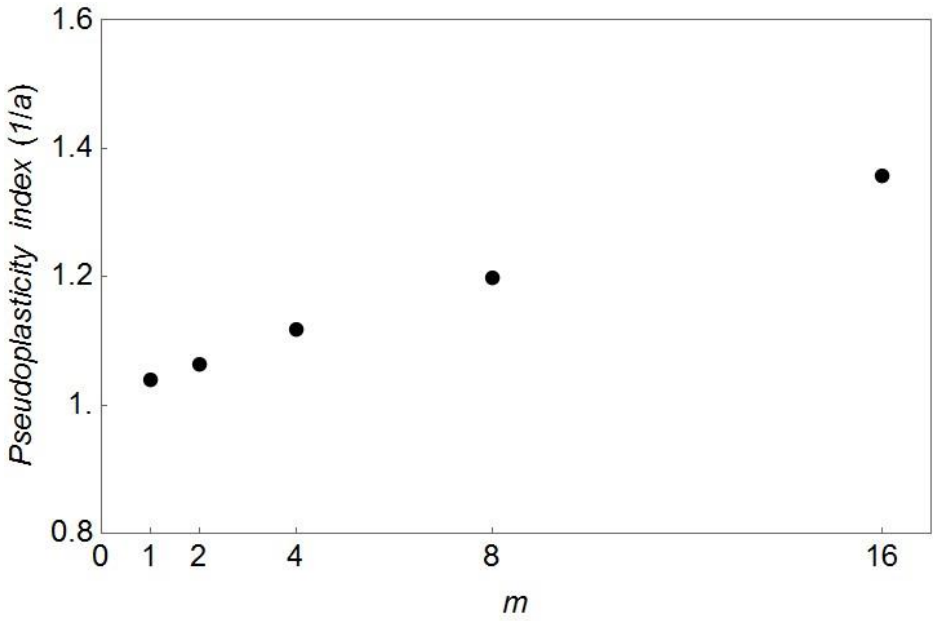

Figure 11. Viscoelasticity of chains as a function of spherical sites

It can be observed that the larger the chains, the more viscoelastic behavior they have and for the first sixteen monomers it follows a linear regression.

In the work of Soto-Castruita et al.,[30] they realized oscillatory experiments with different molecular weight oils (i.e. different chain length oils). They measured the loss and storage moduli at different shear rates and calculated a parameter that quantifies the viscoelasticity of the materials. With that results they proved that viscoelasticity of oils increased as molecular weight increased. In this context, the results obtained in this work, from the molecular point of view, can be used to understand the macroscopic behavior of a fluid.

4. Conclusions

The viscosity and the normal forces for different chains (composed by 1, 2, 4, 8 and 16 spherical sites) were calculated using the reverse non-equilibrium molecular dynamics method. It was presented the role of the normal forces in the shear thinning viscosity at high shear rates and which force dominates the flow behavior depending on the number of sites on the chain. It was proved that the shear flow affects the orientation of molecules and induces an alignment of chains. A relationship between the viscoelastic behavior and the number of sites in the chain was also presented. In conclusion it was found that the normal forces are the responsible of the shear thinning and that they grow up as chains increase in length.

Acknowledgements

Support for this work has been provided by the “Fondo Sectorial SENER-CONACYT-HIDROCARBUROS”, grant no. 186291. Author acknowledges the support of Dr. Sergio E. Quiñones Cisneros and Dr. Ulrich K. Deiters in the realization of this work.

References

1. Macosko, C. W., *Rheology: principles, measurements, and applications*. VCH: 1994.
2. Quiñones-Cisneros, S. E.; Deiters, U. K., Generalization of the Friction Theory for Viscosity Modeling. *The Journal of Physical Chemistry B* **2006,** *110* (25), 12820-12834.
3. Quiñones-Cisneros, S. E.; Zéberg-Mikkelsen, C. K.; Stenby, E. H., The friction theory (f-theory) for viscosity modeling. *Fluid Phase Equilibria* **2000,** *169* (2), 249-276.
4. Pedersen, K. S.; Rønningsen, H. P., Effect of Precipitated Wax on ViscosityA Model for Predicting Non-Newtonian Viscosity of Crude Oils. *Energy & Fuels* **2000,** *14* (1), 43-51.
5. Ramírez-González, P.; Aguayo, J.; Quiñones-Cisneros, S.; Deiters, U., Non-Newtonian Viscosity Modeling of Crude Oils—Comparison Among Models. *International Journal of Thermophysics* **2009,** *30* (4), 1089-1105.
6. Allen, P.; Tildesley, D. J., *Computer Simulation of Liquids*. Clarendon Press: 1989.
7. Toda, M.; Kubo, R.; Saitō, N.; Hashitsume, N., *Statistical Physics II: Nonequilibrium Statistical Mechanics*. Springer Berlin Heidelberg: 1992.
8. Morriss, G. P.; Evans, D. J., *Statistical Mechanics of Nonequilbrium Liquids*. ANU Press: 2013.
9. Hanley, H. J. M.; Evans, D. J., A thermodynamics for a system under shear. *The Journal of Chemical Physics* **1982,** *76* (6), 3225-3232.
10. Ashurst, W. T.; Hoover, W. G., Argon Shear Viscosity via a Lennard-Jones Potential with Equilibrium and Nonequilibrium Molecular Dynamics. *Physical Review Letters* **1973,** *31* (4), 206-208.
11. Delhommelle, J.; Petravic, J.; Evans, D. J., Non-Newtonian behavior in simple fluids. *The Journal of Chemical Physics* **2004,** *120* (13), 6117-6123.
12. Kröger, M., Simple models for complex nonequilibrium fluids. *Physics Reports* **2004,** *390* (6), 453-551.
13. Müller-Plathe, F., Reversing the perturbation in nonequilibrium molecular dynamics: An easy way to calculate the shear viscosity of fluids. *Physical Review E* **1999,** *59* (5), 4894-4898.
14. Bordat, P.; Müller-Plathe, F., The shear viscosity of molecular fluids: A calculation by reverse nonequilibrium molecular dynamics. *The Journal of Chemical Physics* **2002,** *116* (8), 3362-3369.
15. Müller-Plathe, F.; Bordat, P., Reverse Non-equilibrium Molecular Dynamics. In *Novel Methods in Soft Matter Simulations*, Karttunen, M.; Lukkarinen, A.; Vattulainen, I., Eds. Springer Berlin Heidelberg: 2004; Vol. 640, pp 310-326.
16. Johnson, J. K.; Müller, E. A.; Gubbins, K. E., Equation of state for Lennard-Jones chains. *Journal of Physical Chemistry* **1994,** *98* (25), 6413-5419.
17. Galliero, G.; Boned, C., Shear viscosity of the Lennard-Jones chain fluid in its gaseous, supercritical, and liquid states. *Physical Review E* **2009,** *79* (2), 021201.
18. Todd, B. D.; Evans, D. J.; Daivis, P. J., Pressure tensor for inhomogeneous fluids. *Physical Review E* **1995,** *52* (2), 1627-1638.
19. Hoang, H.; Galliero, G., Shear viscosity of inhomogeneous fluids. *The Journal of Chemical Physics* **2012,** *136* (12), -.
20. SCHRAMM, G. A.; Haake, G., *A Practical Approach to Rheology and Rheometry*. Haake: 1994.

21. Barnes, H. A.; Hutton, J. F.; Walters, K., *An Introduction to Rheology*. Elsevier: 1989.
22. Barnes, H. A., *A handbook of elementary rheology*. University of Wales, Institute of Non-Newtonian Fluid Mechanics: 2000.
23. Ramírez-González, P. V.; Quiñones-Cisneros, S. E.; Deiters, U. K., Chemical potentials and phase equilibria of Lennard-Jones chain fluids. *Molecular Physics* **2015,** *113* (1), 28-35.
24. Galliéro, G.; Boned, C.; Baylaucq, A., Molecular Dynamics Study of the Lennard−Jones Fluid Viscosity: Application to Real Fluids. *Industrial & Engineering Chemistry Research* **2005,** *44* (17), 6963-6972.
25. Llovell, F.; Marcos, R. M.; Vega, L. F., Free-Volume Theory Coupled with Soft-SAFT for Viscosity Calculations: Comparison with Molecular Simulation and Experimental Data. *The Journal of Physical Chemistry B* **2013,** *117* (27), 8159-8171.
26. Kröger, M.; Hess, S., Rheological Evidence for a Dynamical Crossover in Polymer Melts via Nonequilibrium Molecular Dynamics. *Physical Review Letters* **2000,** *85* (5), 1128-1131.
27. Evans, M. W.; Heyes, D. M., Correlation functions in non-Newtonian couette flow. A group theory and molecular dynamics approach. *Journal of the Chemical Society, Faraday Transactions* **1990,** *86* (7), 1041-1049.
28. Hess, S., Structure and Nonlinear Flow Behavior of Simple and Complex Fluids. *International Journal of Thermophysics* **2002,** *23* (4), 905-920.
29. Rudolph, N.; Osswald, T. A., *Polymer rheology: fundamentals and applications*. Carl Hanser Verlag GmbH Co KG: 2014.
30. E. Soto, P. V. R.-G., Sergio E. Quiñones-Cisneros, Effect of the Temperature onto the non-Newtonian Behavior of Heavy Oils. *Energy and Fuels* **2014**.